CWE-8
June 7-11, 2026
London, ON, Canada

Influence of wind-wave interaction on turbulent flow structures in large offshore wind farms

Saroj Gautam [a, *], Kevin Pope [a], Baafour Nyantekyi-Kwakye [b], Jahrul M Alam [c]

[a]*Department of Mechanical and Mechatronics Engineering, Memorial University of Newfoundland, St. John's, NL A1C 5S7, Canada, sgautam@mun.ca*
[b]*Department of Mechanical Engineering, Dalhousie University, 1360 Barrington St, PO Box 15000, Halifax, NS B3H 4R2, Canada*
[c]*Department of Mathematics and Statistics, Memorial University of Newfoundland, St. John's, NL A1C 5S7, Canada*

SUMMARY

This study examines the impact of wind-wave interactions on turbulent flow structures, wake recovery, and energy distribution within large offshore wind farms. Large-eddy simulations are performed for a mixed-layout wind farm containing 30 large 15-MW turbines and 20 intermediate 5-MW turbines, arranged in six and five rows, respectively. Two representative drag conditions induced by wind–wave interactions, corresponding to low (R_1) and high (R_2) aerodynamic roughness, are evaluated to compare smooth-sea and rough-sea surface effects at a Reynolds number of $\mathcal{R}_D = 1.6 \times 10^8$. Flow statistics across multiple downstream rows, together with detailed vortex visualizations, are used to identify the multiscale mechanisms that govern wake recovery, turbulence production, and energy redistribution. The findings support the development of improved wind-farm layout design, more reliable turbine performance prediction, and accurate turbulence-resolving models for realistic offshore conditions.

Keywords: *Large-eddy simulation, Offshore wind farm, Turbulence, Wake dynamics, Vortical structures*

1. BACKGROUND AND MOTIVATION

Offshore wind farms operating in a marine atmospheric boundary layer are strongly influenced by wind-wave coupling. Wind-wave interaction in the ocean surface modifies the near-surface shear and turbulence production, which propagate upward into the turbine rotor layer and influence turbine wakes (Porchetta et al., 2021). Large farms often combine turbines of different ratings to optimize energy capture, reduce wake losses, and improve load distribution (Akhtar et al., 2024). In this study, a wind farm with 15 MW and 5 MW turbines is modelled to capture complex interactions, where the stronger wakes from larger turbines affect the performance of smaller downstream turbines. These interactions, coupled with surface-induced turbulence, directly affect power output, fatigue loads, and wake persistence across the farm. In a heterogeneous offshore wind farm with turbines of different ratings, local wake interactions, amplified by surface roughness, dominate the variability of turbine power output and govern the redistribution of energy across the farm (Alam, 2022). This work provides a large eddy simulation, LES, based comparison between the two drag-coefficient regimes (R_1 and R_2) to assess the influence of sea-state-dependent surface forcing on wake breakdown, vortex stretching, turbulence anisotropy, and energy transfer in heterogeneous offshore wind farms.

2. NUMERICAL FORMULATION

The present study employs LES of an offshore wind farm with 50 full-scale wind turbines, each represented using an actuator-disk formulation. The simulations resolve a neutrally stratified, incompressible marine atmospheric boundary layer (ABL), modeled using the filtered momentum and continuity equations under a constant-density assumption given by,

$$\frac{\partial \tilde{u}_i}{\partial x_j} = 0 \tag{1}$$

$$\frac{\partial \tilde{u}_i}{\partial t} + \tilde{u}_j \frac{\partial \tilde{u}_i}{\partial x_j} = -\frac{1}{\rho_0}\frac{\partial \tilde{p}}{\partial x_i} - \frac{\partial \tau_{ij}}{\partial x_j} + f_i \tag{2}$$

Where $\tilde{u}_i$ and $\tilde{p}$ are the filtered velocity and pressure fields, f_i is the turbine-induced body force, and τ_{ij} is the subfilter-scale (SFS) stress tensor. The filtering operation is applied implicitly through the numerical discretization, so that the unresolved motions smaller than the grid scale are represented by the SFS stress tensor,

$$\tau_{ij} = \widetilde{u_i u_j} - \tilde{u}_i \tilde{u}_j \tag{3}$$

The SFS stress is decomposed into its isotropic and deviatoric parts. The deviatoric component is modeled following a Deardorff-type formulation:

$$\tau_{ij} - \frac{1}{3}\tau_{kk}\delta_{ij} = c_k \Delta_{LES} \sqrt{k_{sgs}} \mathcal{S}_{ij} \tag{4}$$

Where $\mathcal{S}_{ij} = \left(\partial_j \tilde{u}_i + \partial_i \tilde{u}_j\right)/2$ is the resolved strain rate. The SGS kinetic energy k_{sgs} is given by the local velocity-gradient invariants using

$$k_{sgs} = \Delta^2 \mathcal{I}_1^{1/3} (\mathcal{I}_2)^{-2/3} \tag{5}$$

With $\mathcal{I}_1 = \frac{1}{2}\mathcal{S}_{ij}\omega_j \mathcal{S}_{ik}\omega_k + \frac{1}{6}\left(\mathcal{G}_{ij}\mathcal{G}_{ji}\right)^2, \mathcal{I}_2 = \left(\mathcal{S}_{ij}\mathcal{S}_{ij}\right)^{5/2} + \mathcal{I}_1^{5/2}$, $\omega_i = \epsilon_{ijk}\,\partial_j \tilde{u}_k, \mathcal{G}_{ij} = \partial_j \tilde{u}_i$.

To ensure dynamic consistency between the subgrid-scale viscosity and the resolved flow, the model is coupled with a simplified transport equation for k_{sgs}, providing stable and physically accurate simulations of offshore wind farms and the marine atmospheric boundary layer. The sea surface is modeled using a wall-stress formulation with two roughness heights representing low- and high-roughness sea states. This approach captures their impact on momentum flux, boundary-layer structure, and wake development. The sea surface is modeled using a wave-dependent aerodynamic roughness formulation similar to Zhang et al. (2024). To capture sea-state variability, two rough-sea conditions with corresponding drag coefficients are specified and used in the simulations.

3. NUMERICAL MODEL AND PRELIMINARY FLOW CHARACTERISTICS

The incompressible filtered Navier–Stokes equations are solved on a structured grid with 200 million cells, using inlet-outlet conditions in the streamwise direction, symmetry on the top and cyclic spanwise boundaries to emulate an extended wind farm as shown in Fig.1(a). Turbines are modelled as actuator disks applying spatially filtered body forces consistent with classical momentum theory. All simulations are performed on Compute Canada clusters using 1,536 processors.

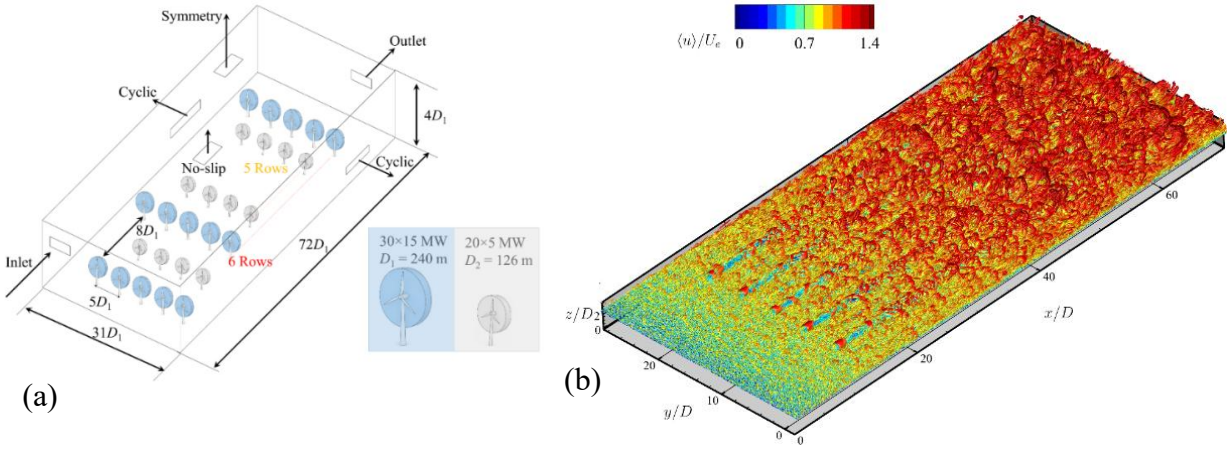

Figure 1. (a) Schematic of the wind farm turbine arrangement and boundary conditions. (b) Vortex structures identified by Q-criterion and colored by normalized mean streamwise velocity $\langle u \rangle / U_e$. Spiral tip vortices are visible near the turbines, transitioning to broken vortex tubes and "horseshoe" vortices in the far wake due to increased turbulence. Spatial distances are normalized by the 15 MW turbine rotor diameter, and velocity is normalized by the free-stream velocity, U_e.

Figure 1(b) shows a stream tube originating from the first five rows of turbines, colored by mean velocity. Wake vortices develop downstream, with mixing becoming prominent in the far wake. Coherent vortical structures are visualized using the Q-criterion, defined as, $Q = 1/2(\|\Omega\|^2 - \|S\|^2)$, where Ω and S are the rotation and strain-rate tensors, respectively. Regions with $Q > 0$, highlight the evolution of vortical structures and interactions within the turbine wakes.

Figure 2 shows the wake characteristics behind the first rows of 15 MW and 5 MW turbines. The first-row wakes exhibit the largest velocity deficit, which partially recovers in the second row. Wind–wave-induced drag amplifies turbulent fluctuations, as seen in $\overline{u'^2}, \overline{v'^2}, \& \overline{w'^2}$ profiles Fig.2(d-f), enhancing mixing and momentum transfer in the near-wake region. The increased turbulence downstream of the first row affects the wake structure encountered by the smaller second-row turbines, influencing their velocity deficit, turbulence, and their power production.

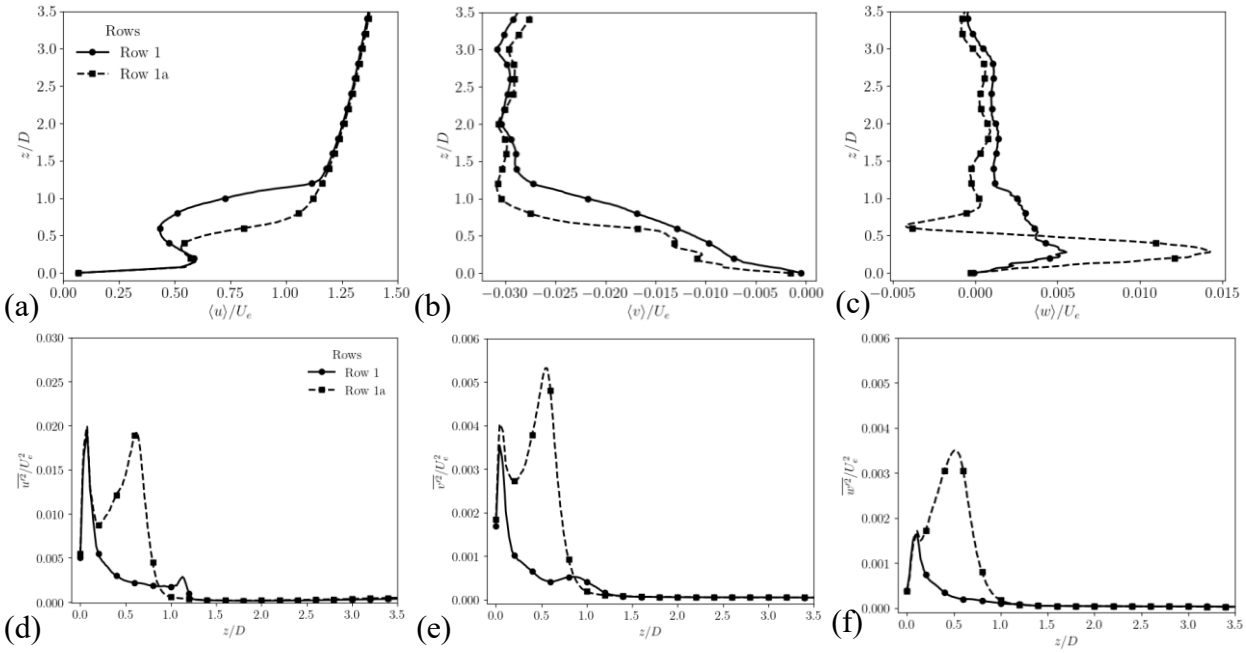

Figure 2. Profiles of mean velocity components (top) and velocity fluctuations (bottom) at the first two rows of the wind farm. Mean velocity components $\langle u \rangle$, $\langle v \rangle$ and $\langle w \rangle$ are normalized by the free-stream velocity U_e, while fluctuations $\overline{u'^2}$, $\overline{v'^2}$ and $\overline{w'^2}$ are normalized by U_e^2. The vertical location is normalized by the 15 MW rotor diameter. The solid black line with circle markers (●—) represents Row 1 with 15 MW turbines, and the dashed black line with square markers (■- -) represents Row 1a with 5 MW turbines.

4. CONCLUSIONS

This study will provide a comprehensive quantification of the influence of sea-state-dependent drag on flow dynamics, wake interactions, and energy transfer in large offshore wind farms. The results will reveal the trends in wake recovery, turbulence generation, vortex evolution, and energy distribution across the farm, providing insights into turbine performance under different surface conditions. These outcomes will support improved wind-farm layout design and more accurate power prediction in offshore wind farms.

ACKNOWLEDGEMENTS

The authors gratefully acknowledge financial support from Natural Sciences and Engineering Research Council of Canada (NSERC), and computational resources provided by the Digital Research Alliance of Canada.

REFERENCES

Akhtar, N., Geyer, B., Schrum, C., 2024. Larger wind turbines as a solution to reduce environmental impacts. Sci Rep 14, 6608. https://doi.org/10.1038/s41598-024-56731-w

Alam, J., 2022. Interaction of vortex stretching with wind power fluctuations. Physics of Fluids 34, 075132. https://doi.org/10.1063/5.0099347

Porchetta, S., Muñoz-Esparza, D., Munters, W., Van Beeck, J., Van Lipzig, N., 2021. Impact of ocean waves on offshore wind farm power production. Renewable Energy 180, 1179–1193. https://doi.org/10.1016/j.renene.2021.08.111

Zhang, C., Chen, L., Brett, M.T., 2024. Adaptation of Wind Drag Coefficient Parameterization: Improvement of Hydrodynamic Modeling by a Wave-Dependent C_d in Large Shallow Lakes. Water Resources Research 60, e2023WR035914. https://doi.org/10.1029/2023WR035914